Journal of Arrhythmia 33 (2017) 447–454

Contents lists available at ScienceDirect

Journal of Arrhythmia

journal homepage: www.elsevier.com/locate/joa

Original Article

Scar characteristics derived from two- and three-dimensional reconstructions of cardiac contrast-enhanced magnetic resonance images: Relationship to ventricular tachycardia inducibility and ablation success

Kazumasa Sonoda, Yasuo Okumura*, Ichiro Watanabe, Koichi Nagashima, Hiroaki Mano, Rikitake Kogawa, Naoko Yamaguchi, Keiko Takahashi, Kazuki Iso, Kimie Ohkubo, Toshiko Nakai, Satoshi Kunimoto, Atsushi Hirayama

Division of Cardiology, Department of Medicine, Nihon University School of Medicine, 30-1 Ohyaguchi kami-cho, Itabashi-ku, Tokyo 173-8610, Japan

ARTICLE INFO

Article history:
Received 24 August 2016
Received in revised form
26 October 2016
Accepted 15 November 2016
Available online 31 December 2016

Keywords:
Ventricular tachycardia
Structural heart disease
Contrast-enhanced cardiac magnetic resonance

ABSTRACT

Background: The relationship between cardiac contrast-enhanced magnetic resonance imaging (CE-MRI)-derived scar characteristics and substrate for ventricular tachycardia (VT) in patients with structural heart disease (SHD) has not been fully investigated.
Methods: This study included 51 patients (mean age, 63.3 ± 15.1 years) who underwent CE-MRI with SHD and VT induction testing before ablation. Late gadolinium-enhanced (LGE) regions on MRI slices were quantified by thresholding techniques. Signal intensities (SIs) 2–6 SDs above the mean SI of the remote left ventricular (LV) myocardium were considered as scar border zones, and SI > 6 SDs, as scar zone, and the scar characteristics related to VT inducibility and successful ablation via endocardial approaches were evaluated.
Results: The proportion of the total CE-MRI-derived scar border zone in the inducible VT group was significantly greater than that in the non-inducible VT group (26.3 ± 9.9% vs. 19.2 ± 7.8%, respectively, $P=0.0323$). The LV endocardial scar zone to total LV myocardial scar zone ratio in patients whose ablation was successful was significantly greater than that in those whose ablation was unsuccessful (0.61 ± 0.11 vs. 0.48 ± 0.12, respectively, $P=0.0042$). Most successful ablation sites were located adjacent to CE-MRI-derived scar border zones.
Conclusions: By CE-MRI, we were able to characterize not only the scar, but also its location and heterogeneity, and those features seemed to be related to VT inducibility and successful ablation from an endocardial site.

1. Introduction

Ventricular tachycardia (VT) occurring in the presence of structural heart disease (SHD) can be fatal. The main mechanism of VT is reentry, and the circuits exist mainly in or adjacent to scar border zones. The critical isthmus of the VT circuit is often located within the scar or scar border zones, and such isthmus can be identified in three-dimensional (3D) electroanatomic maps created during entrainment mapping of VT and upon mapping delayed or fragmented potentials and/or pace mapping performed during the sinus rhythm [1,2]. The critical isthmus of the VT circuit has been used as the target for ablation. However, VT ablation remains challenging, particularly in patients with nonischemic cardiomyopathy or arrhythmogenic right ventricular cardiomyopathy (ARVC) because epicardial ablation is often required to eliminate critical VT circuits [3]. Therefore, determining whether VT can be ablated from the left ventricular (LV) endocardium before the procedure in patients with SHD is clinically important. Cardiac contrast-enhanced magnetic resonance imaging (CE-MRI) with late gadolinium enhancement (LGE) is a robust tool for detecting fibrosis in patients with SHD [4–10]. Scar distribution and heterogeneity can also be identified by CE-MRI [4,11,12]. Heterogeneous scar tissue results in slow conduction and becomes the substrate for reentrant VT [10]. We, therefore, conducted a study to examine the relationship between the scar characteristics revealed by CE-MRI and VT inducibility, and the ablation outcomes.

2. Materials and methods

2.1. Study population

The study group comprised 51 consecutive patients (42 men, 9 women; mean age, 63.3 ± 15.1 years) with SHD and VT who underwent electrophysiologic study and CE-MRI before ablation therapy between September 2007 and May 2015. In all 51 patients,

* Corresponding author. Fax: +81 3 3972 1098.
E-mail address: yasuwo128@yahoo.co.jp (Y. Okumura).

http://dx.doi.org/10.1016/j.joa.2016.11.001

the VTs were documented by ambulatory electrocardiography (ECG), 12-lead ECGs, or 24-h Holter ECG monitoring. The patients' SHD resulted from remote myocardial infarctions ($n=20$), cardiac sarcoidosis ($n=12$), hypertrophic cardiomyopathy ($n=10$), ARVC ($n=3$), dilated cardiomyopathy ($n=4$), or cardiomyopathy of unknown etiology ($n=2$). Patients for whom CE-MRI was contraindicated, including those with pacemakers or defibrillators, those with stage IV/V chronic kidney disease, or those unable to lie flat, were excluded. The study protocol was approved by our institutional review board, and all patients provided written informed consent for their participation.

2.2. ECG criteria for the QRS fragmentation

The RSR′ pattern included various QRS interval morphologies (QRS duration <120 ms) with or without Q waves. Fragmentation inside the QRS was defined by the presence of an additional R wave (R′) or notching in the nadir of the S wave or the presence of >1 R′ (fragmentation) in two contiguous leads. A typical bundle-branch block pattern (QRS >120 ms) and incomplete right bundle-branch block were excluded from the study [13].

2.3. CE-MRI protocol

All CE-MRI were obtained with a 1.5-T MR scanner (Achieva, Philips Medical Systems, Best, The Netherlands) using five-channel SENSE cardiac coils. Scout images were acquired initially to determine the cardiac axes. ECG-gated breath-hold steady- state free precession cine images were obtained in two-, three-, and four-chamber views, and in 2.5-mm short-axis slices from the base to the apex. A gadolinium-based contrast agent (0.2 mmol/kg, Gadovist, Schering, Berlin, Germany) was administered intravenously, and a breath-hold segmented inversion recovery gradient echo sequence was obtained 10 min after the contrast injection and in the same orientation as the cine images [4–12]. The slices were matched as closely as possible to those obtained for the cine and LGE sequences.

2.4. Image analysis

All CMR images were analyzed by electrocardiologists blinded to the results of the electrophysiologic evaluations. The LV endocardium and epicardium were traced manually on the short-axis slices obtained at end diastole (Ziostation 2 software, Ziosoft, *Tokyo,Japan*). All short-axis slices covering the entire LV were inspected visually to identify the normal myocardium (Fig. 1**A**), which was taken as the region with no contrast enhancement and normal wall thickness. A region of interest (ROI) in the normal area was planimetered, and the mean signal intensity (SI) and standard deviation (SD) of the SI were calculated (Fig. 1**B**, upper panel). Thereafter, any area of hyperenhancement was identified and outlined. A scar zone was defined by a specific SI threshold, i.e., an SI of >6 SD of the normal area [5,8,9] and displayed in red, whereas a scar border zone was defined by an SI of >2 SD and ≤ 6 SD of the normal area and displayed in yellow (Fig. 1A, B lower panel) [9,14]. Summing the planimetered areas in all LGE slices yielded the total masses of the scar and scar border zones, and those were expressed as percentages of the total LV myocardium (%scar and %scar border zones) [11,12] (Supplemental file). Two ratios, representing the scar and scar border zones on the endocardial side of the LV, were calculated as follows: scar zone (g) in the LV endocardium/total LV myocardial scar zone (g) and scar border zone in the LV endocardium (g)/total LV myocardial scar border zone (g), respectively (Fig. 1C). The endocardial side of the LV was defined as the LV endocardium, including the LV myocardium up to 50% of its thickness. For the 10 most recently enrolled patients, 3D-reconstructed CE-MR images of the LV were also created with the use of custom software (M.I. Systems, Kobe, Japan) (Supplemental file).

2.5. VT induction and catheter ablation

Electrophysiologic studies and ablation were performed under sedation achieved with midazolam and fentanyl. A 6-Fr quadripolar catheter was introduced via the right femoral vein and placed across the tricuspid valve to record His bundle electrograms, and a second 7-Fr quadripolar catheter was introduced similarly and placed in the right ventricular (RV) apex for pacing. VT was induced from the RV apex and outflow tract by delivering single, double, or triple extra stimuli during basic cycle lengths of 400 and 600 ms. The same steps were taken under isoproterenol infusions (0.25 μg/min) if VT was not induced by programmed stimulation. Inducible VT was defined as induction of sustained monomorphic VT that lasted ≥ 30 s or that requiring cardioversion because of hemodynamic compromise. Mapping was performed in the RV or LV, depending on the morphology of the targeted ventricular arrhythmias. Intravenous heparin was administered to maintain an activated clotting time of >250 s and >200 s during LV and RV mapping, respectively. Electroanatomical voltage mapping was performed with a 3.5-mm irrigated-tip catheter (1-mm ring electrode, 2-mm interelectrode spacing; NaviStar ThermoCool, Biosense Webster Inc, Diamond Bar, CA, USA) and CARTO system (Biosense Webster Inc., Diamond Bar, CA, USA). Intracardiac electrograms were filtered at 30–500 Hz (bipolar) and 1–250 Hz (unipolar). In cases of hemodynamically stable VT, potential re-entry circuit sites targeted for ablation were identified based on activation and entrainment mapping. The potential ablation sites were identified by substrate and pace mapping for unstable VTs. Low voltages were defined as bipolar voltage amplitudes of <1.5 mV, with scar defined as <0.5 mV and scar borders as 0.5–1.5 mV. Fractionated and delayed potentials were mapped from the LV endocardium at bipolar voltages of <1.5 mV. For analysis purposes, RF ablation target sites were defined as sites with (1) good pace maps, i.e., matching surface morphologies in 11/12 electrogram leads, or (2) a critical isthmus identified by concealed entrainment and a post-pacing interval equal to the VT cycle length, or (3) VT termination during ablation. Radiofrequency power output was initially set at 30 W and increased up to 40 W. Ablation was performed during VT in patients with hemodynamically stable VT and during sinus rhythm in patients with hemodynamically unstable VT to target all fractionated and/or delayed potentials. Programmed stimulation was repeated after ablation, and successful catheter ablation was defined as non-inducibility of sustained monomorphic VT.

2.6. Statistical analysis

Continuous variables were expressed as the mean $\pm$ SD. Between-group differences in continuous variables, including clinical, electrocardiographic, and echocardiographic variables, were analyzed by an unpaired t test or Mann–Whitney U test, as appropriate. Categorical variables are expressed as percentages, and between-group differences were analyzed by a Fisher exact test. All statistical analyses were performed with JMP 9 software (SAS Institute, Cary, NC, USA), and $P<0.05$ was considered statistically significant.

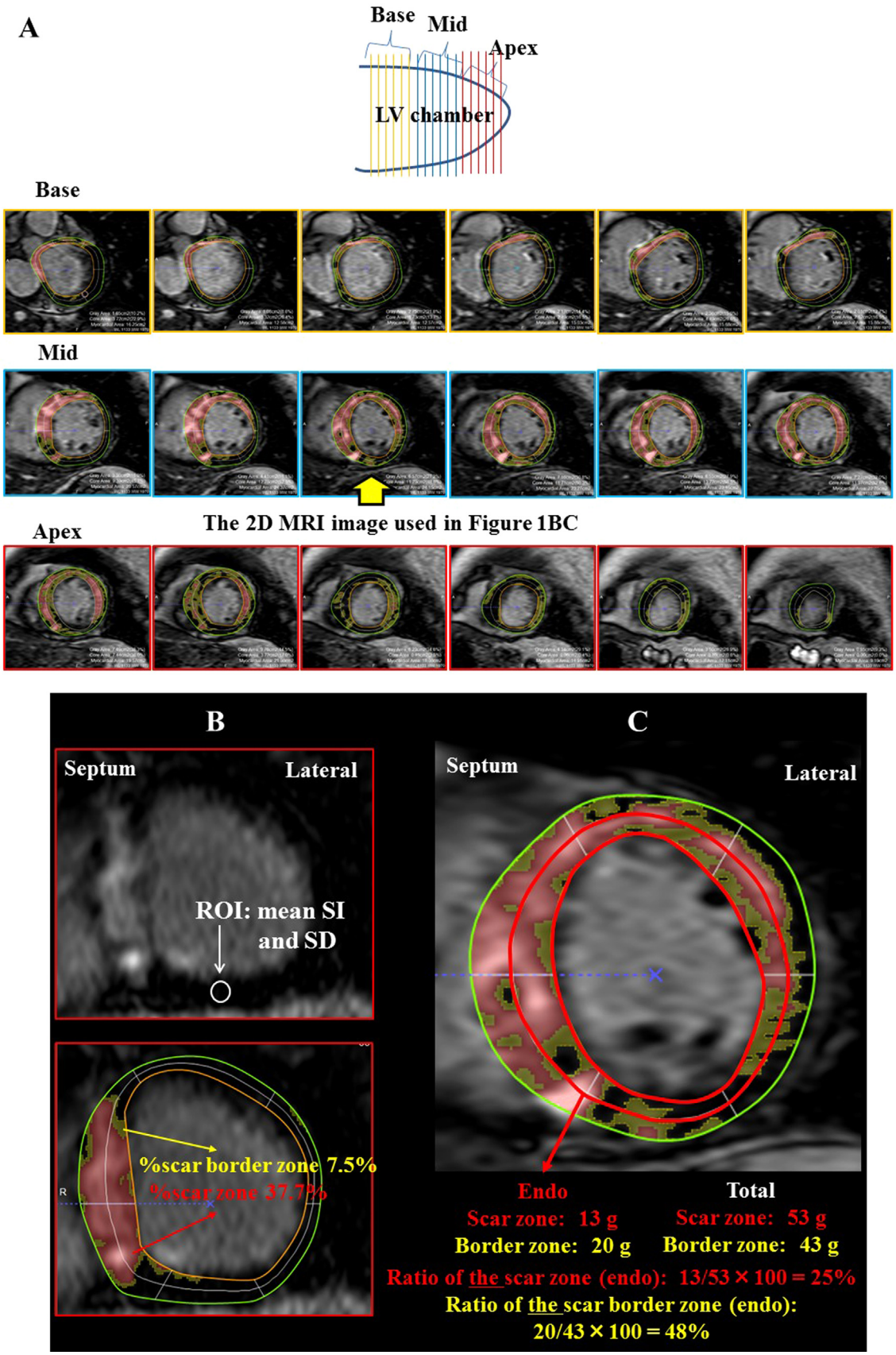

Fig. 1. Representative quantification of scar and scar border zones on 2D CE-MRI. (A) The whole left ventricular (LV) slices of 2D CE-MR images. (B) A region of interest (ROI) in the remote normal myocardium is determined by the reader, and the mean ± SD of the signal-intensity (SI) of the ROI are automatically calculated. An algorithm applies SI thresholds of 6 SDs and 2–6 SDs above the SI of the remote normal myocardium to delineate the scar zone (red region) and scar border zone (yellow region), respectively. The total mass of the scar zone and scar border zone (g), and their percentages relative to total myocardium (%scar zone and %scar border zone) are automatically calculated. (C) The LV endocardium is manually outlined, and areas of late gadolinium enhancement (LGE) on all short-axis slices are planimetered and yield the total masses of the scar and scar border zones (g), and the LV endocardial scar zone (g)/total LV myocardial scar zone (g) ratio and LV endocardial scar border zone (g)/total LV myocardial scar border zone (g) ratio are calculated.

3. Results

3.1. Baseline characteristics

Seventy-two sustained monomorphic VTs (1.7 ± 1.1 VTs per patient; VT cycle length: 310 ± 29 ms) were induced in 40 of 51 patients, and not in the remaining 11. The patients' clinical, electrocardiographic, and echocardiographic characteristics are shown per group in Table 1. Male sex and no use of statins in the inducible VT group tended to be more prevalent than that in non-inducible VT group. No differences were found in the other clinical variables, including the LVEF, between the two groups.

Table 1
Clinical characteristics and electrocardiographic and echocardiographic variables per study group.

	Inducible VT (n=40)	Non-inducible VT (n=11)	P value*
Age (years)	62.7 ± 15.4	65.6 ± 14.2	0.5691
Male sex	35 (88)	7 (64)	0.0868
Clinical history			
Diabetes mellitus	13 (33)	1 (9)	0.2508
Hypertension	28 (73)	8 (73)	> 0.9999
Medication use			
ACE-I/ARB	23 (58)	5 (45)	0.5137
Antiplatelet	17 (43)	6 (55)	0.5137
Beta-blocker	21 (53)	6 (55)	> 0.9999
Statin	20 (50)	9 (82)	0.0877
Antiarrhythmic class III	19 (48)	5 (45)	> 0.9999
Underlying heart disease			
RMI	13 (33)	7 (64)	0.3599
HCM	9 (23)	1 (9)	
DCM	4 (10)	0 (0)	
CS	9 (23)	3 (27)	
ARVC	3 (8)	0 (0)	
Unknown	2 (5)	0 (0)	
NYHA functional class			
I	23 (58)	8 (73)	
II	11 (28)	3 (27)	0.3717
III or more	6 (15)	0 (0)	
ECG			
Heart rate (beats/min)	68 ± 12	71 ± 20	0.5927
Normal sinus rhythm	38 (95)	10 (91)	0.5256
QRS duration	115 ± 26	100 ± 9	0.0836
Right bundle branch block	6 (15)	1 (9)	> 0.9999
Left bundle branch block	1 (3)	0 (0)	> 0.9999
QRS fragmentation	18 (45)	3 (27)	0.4905
Echocardiography			
LAD (mm)	40.2 ± 8.6	39.0 ± 6.7	0.6624
LVDd (mm)	54.9 ± 10.4	53.7 ± 9.5	0.7134
LVDs (mm)	39.6 ± 11.2	39.7 ± 12.0	0.9640
LVEF (%)	46.5 ± 16.6	51.9 ± 19.1	0.3510
IVSd (mm)	10.8 ± 3.6	10.2 ± 1.6	0.5508
PWd (mm)	10.3 ± 2.4	9.6 ± 1.8	0.3712
E/A	1.2 ± 0.8	1.0 ± 0.6	0.4798
E/e′	12.9 ± 6.0	12.1 ± 5.0	0.6809

Values are presented as mean ± SD, or n (%).
RMI, remote myocardial infarction; HCM, hypertrophic cardiomyopathy; DCM, dilated cardiomyopathy; CS, cardiac sarcoidosis; ARVC, arrhythmogenic right ventricular cardiomyopathy; ECG, electrocardiography; NYHA, New York Heart Association; LAD, left atrial diameter; LVDd, left ventricular end diastolic dimension; LVDs, left ventricular end systolic dimension; LVEF, left ventricular ejection fraction; IVSd, interventricular septal end diastolic dimension; PWd, left ventricular posterior end diastolic wall thickness.

3.2. Scar characteristics in the inducible and non-inducible VT groups

No between-group differences were found in the %scar zones calculated from the CE-MR images (24.5 ± 15.2% vs. 22.6 ± 13.4%, P=0.7067), but the %scar border zones in the inducible VT group were significantly greater than that in the non-inducible VT group (26.3 ± 9.9% vs. 19.2 ± 7.8%, P=0.0323) (Fig. 2A). Interestingly, the patients with fragmentation inside the QRS in the 12-lead ECG tended to have a larger %scar zone (29.7 ± 16.3% vs. 20.9 ± 10.7% P=0.0629) than those without, but no association was observed for %scar border zone (26.0 ± 10.7% vs. 24.0 ± 9.8% P=0.5481).

3.3. Scar characteristics and results of LV ablation performed on the endocardial side

Among the 40 patients in whom VT was induced, 29 achieved VT termination and non-inducibility. In the remaining 11 patients, VTs remained inducible (unsuccessful ablation group) at the end of the procedure, most likely because the origin was located in the epicardial side or in the subendocardium. The successful ablation site was located in the RV endocardium (n=7) or LV outflow tract (n=4) in 11 of 29 patients in whom VT termination was achieved. Those 11 patients were excluded from the final analysis because LV fibrosis could not be assessed on their CE-MRI images. Thus, the final successful ablation group comprised 18 patients in whom VT was successfully ablated from the LV endocardium. Representative examples of 2D and 3D CE-MRI images and 3D voltage maps of the LV endocardium obtained in patients with successful and unsuccessful ablation are shown in Figs. 3 and 4.

Clinical characteristics and ECG and echocardiographic variables are shown for the successful and unsuccessful ablation groups in Table 2. No differences were found in the ECG variables between the two groups. As expected, remote myocardial infarctions and the use of antiplatelet drugs in the successful group were significantly more prevalent than those in the unsuccessful ablation group (78% vs. 9%, P=0.0014). NYHA class I was significantly less prevalent in the successful than in the unsuccessful ablation group (44% vs. 91%, P=0.0372). The interventricular septal end-

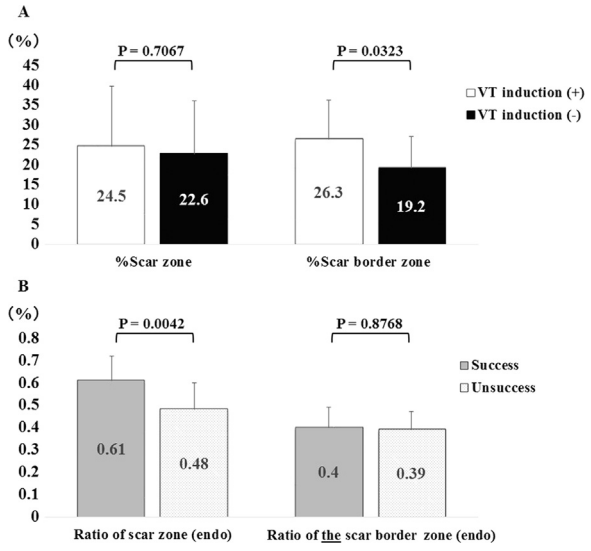

Fig. 2. Bar graphs showing the (A) %scar zone and %scar border zone in the VT inducible and non-inducible groups and (B) scar zone (g) in the LV endocardium/total LV myocardial scar zone (g) ratio and scar border zone in the LV endocardium (g)/total LV myocardial scar border zone (g) ratio in the patient group with successful ablation via the endocardial side of the LV and the patient group unsuccessful ablation. The bars show the mean percentages and ratios per zone.

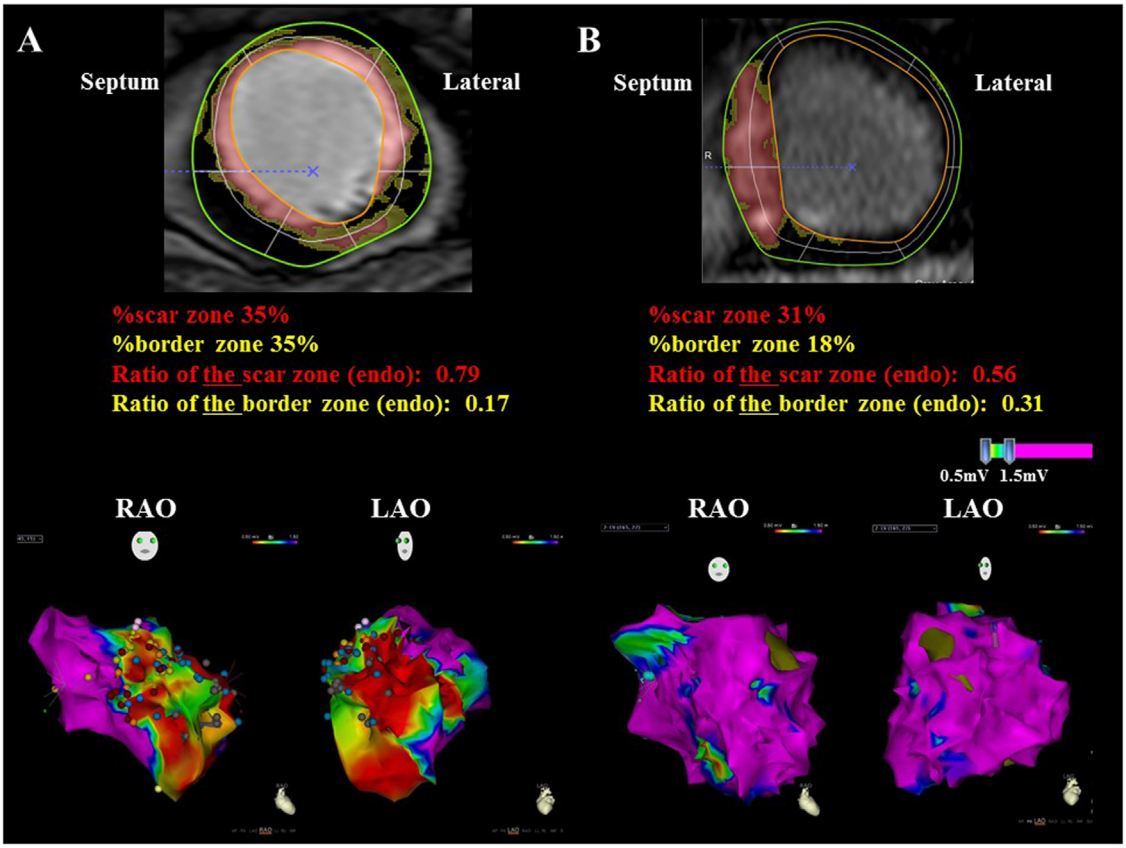

Fig. 3. Representative examples of 2D CE-MR images and 3D endocardial LV voltage maps obtained from (A) patients in whom ablation via the endocardium was successful and (B) patients in whom it was not successful. In the case of successful ablation (A), the CE-MRI-derived scar zone is widely distributed on the endocardial side of the LV (upper panel), which corresponds to the low voltage area on the 3D endocardial LV voltage map (lower panel). In contrast, in the case of unsuccessful ablation (B), the CE-MRI-derived scar zone is located mainly at the mid portion of the LV myocardium (upper panel), and thus, only a small low voltage area is noted at the apical septal wall on the 3D endocardial LV voltage map. The %scar zones in cases of successful and unsuccessful ablation are similar (35% and 31%, respectively), but the LV endocardial scar zone to total LV myocardial scar zone ratio was significantly greater in the successful ablation group than in the unsuccessful ablation group (0.79 vs. 0.56. respectively).

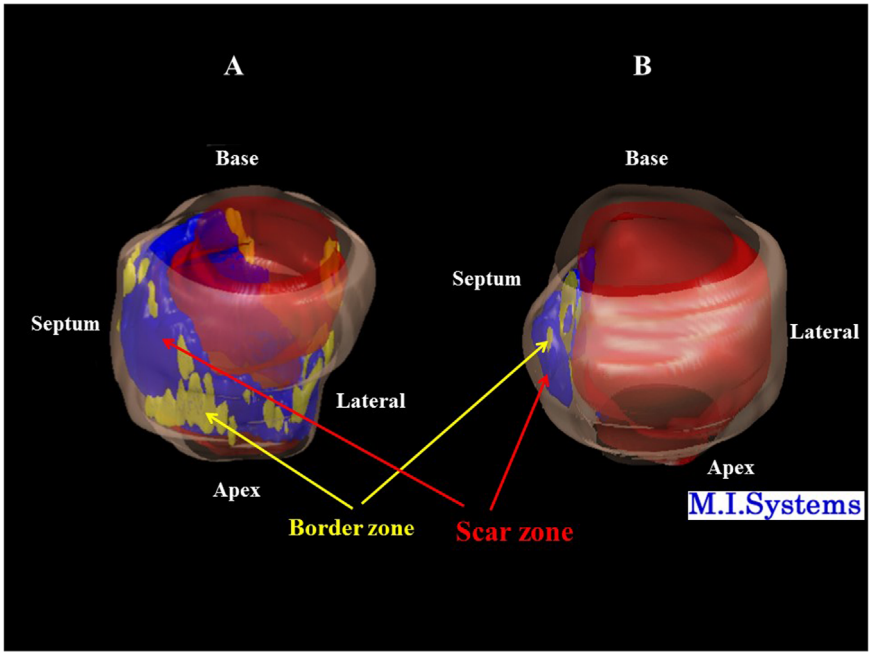

Fig. 4. Representative examples of 3D reconstructed CE-MR images in the cases shown in Fig. 3 wherein ablation via the endocardial side was (A) successful and (B) unsuccessful. The 3D LV reconstructions are derived from short-axis slices of the 2D CE-MRI dataset with the use of custom software. The scar and scar border zones are indicated in blue and yellow, respectively. Note that the distribution of the scar and scar border zones on the 3D CE-MR images can be deduced from the 3D endocardial LV voltage maps shown in Fig. 3.

Table 2
Clinical characteristics and electrocardiographic and echocardiographic variables in patients with successful or unsuccessful ablation from the endocardium.

	Successful ablation ($n=18$)	Unsuccessful ablation ($n=11$)	P value*
Age (years)	65.7 ± 11.5	59.3 ± 18.6	0.2617
Male sex	17 (94)	9 (81)	0.5394
Clinical history			
Diabetes mellitus	5 (28)	2 (18)	0.6765
Hypertension	16 (89)	7 (64)	0.1638
Medication use			
ACE-I/ARB	9 (50)	5 (45)	> 0.9999
Antiplatelet	14 (78)	3 (27)	0.0177
Beta-blocker	12 (67)	3 (27)	0.0604
Statin	11 (61)	5 (45)	0.4657
Antiarrhythmic class III	9 (50)	7 (63)	0.7021
Underlying heart disease			
RMI	**14 (78)**	**1 (9)**	**0.0014**
HCM	**0 (0)**	**5 (45)**	
DCM	**1 (6)**	**0 (0)**	
CS	**3 (17)**	**4 (36)**	
ARVC	**0 (0)**	**1 (9)**	
Unknown	**0 (0)**	**1 (8)**	
NYHA functional class			
I	**8 (44)**	**10 (91)**	
II	**5 (28)**	**1 (9)**	**0.0372**
III or more	**5 (28)**	**0 (0)**	
ECG			
Heart rate (beats/min)	72.1 ± 11.9	68.2 ± 9.8	0.3726
Normal sinus rhythm	15 (83)	11 (100)	0.2154
QRS duration	106.8 ± 22.1	117.4 ± 20.3	0.2080
Right bundle branch block	1 (6)	2 (18)	0.5394
Left bundle branch block	0 (0)	0 (0)	> 0.9999
QRS fragmentation	9 (50)	5 (45)	0.5579
Echocardiography			
Left atrial diameter (mm)	40.3 ± 7.9	40.4 ± 7.2	0.9973
LVDd (mm)	57.6 ± 11.2	56.9 ± 11.0	0.8723
LVDs (mm)	44.4 ± 12.1	42.7 ± 11.5	0.7252
LVEF (%)	40.0 ± 17.0	45.3 ± 13.6	0.3880
IVSd (mm)	9.4 ± 1.9	11.2 ± 2.3	0.0279
PWd (mm)	9.2 ± 2.6	10.6 ± 2.5	0.1716
E/A	1.1 ± 0.6	1.1 ± 0.5	0.8282
E/e′	13.9 ± 6.8	13.5 ± 6.4	0.9015

Values are presented as mean ± SD, or *n* (%).Abbreviations are shown in Table 1.

diastolic dimension (IVSd) in the successful ablation group was significantly smaller than that in the unsuccessful ablation group (9.4 ± 1.9 mm vs. 11.2 ± 2.3 mm, $P=0.0279$).

In analyzing scar characteristics, we found no difference between the successful and unsuccessful ablation groups in the % scar zone or %scar border zone (31.0 ± 13.7% vs. 27.8 ± 17.1%, respectively, P=0.5908; and 24.6 ± 12.4% vs. 21.8 ± 9.6%, respectively, P=0.5284). However, the LV endocardial scar zone to total LV myocardial scar zone ratio in the successful ablation group was significantly greater than that in the unsuccessful ablation group (0.61 ± 0.11 vs. 0.48 ± 0.12, respectively, P=0.0042) (Fig. 2**B**). Successful VT termination sites were located mainly within or adjacent to the scar border zones in the 18 patients in the successful ablation group (Fig. 5**A,B**), but successful ablation sites were located within the scar zone in two patients.

4. Discussion

4.1. Main study findings

The present study yielded three main findings: (1) VT inducibility was related to an increased %scar border zone derived from CE-MR images, indicating an arrhythmogenic substrate, (2) the LV endocardial scar zone to total LV myocardial scar zone ratio was significantly greater in the group of patients for whom VT was successfully eliminated by LV ablation on the endocardial side, and (3) most successful ablation sites were located adjacent to scar border zones.

4.2. Relation between VT induction and CE-MRI-derived scar characteristics

Scar tissue is a critical component of the anatomical substrate for VT in patients with SHD. Regions of scar tissue that incorporate surviving myocardial tissue can include a slow conduction zone in the reentrant circuit and can be ideal VT ablation targets [1,2]. There is growing evidence that CE-MRI allows differentiation between normal myocardium and such scar tissue. In the present study, we could characterize dense and heterogeneous scar tissues, i.e., scar border zones identified by regions of intermediate-intensity contrast enhancement. Two main approaches to CE-MRI-based tissue characterization have been reported: one based on an SI more than that of the remote normal myocardium and the other based on the measured full width at half maximum (FWHM), by which the threshold is considered as 50% of the maximum signal within the scar. Several studies have shown contradicting findings. One group of investigators recommended an SI above 2 SDs from the remote normal myocardium [13]. Beek et al. [8] studied thresholds of 2–8 SDs above the mean SI and FWHM threshold and correlated the infarct size with viability after revascularization. The most predictive SI threshold was 6 SDs, but it was not statistically superior to any other method. Spiewak et al. [5] also found, in a study limited to hypertrophic cardiomyopathy patients, that 6 SDs above the mean SI of the remote myocardium was most comparable to visual assessment of LGE. Furthermore, a validation study comparing SD- and FWHM-thresholding methods against manual quantification confirmed overestimation of the 2 SD technique and showed that manual quantification, 5 or 6 SDs above the mean remote SI, and FWHM thresholding, yielded similar volumes [9]. In light of these reported findings, we accepted > 6 SDs from the mean SI of the remote myocardium as dense scar tissue, i.e., the scar zone, and accepted an SI between 2 SDs and 6 SDs above the mean remote SI as the scar border zone.

We found association between a relatively large scar border zone and VT inducibility. The role of the scar border zone in reentrant VT has been well documented in both animal and human studies [15–17]. In brief, studies have shown that the reentry pathway of VT exists within bands of surviving muscle fibers bordered by dense fibrotic tissue [16–18]. Our finding of a relatively large heterogeneous zone susceptible to VT reinforces this reported pathophysiology explaining the mechanism of reentrant VT. Several reports have also shown that CE-CMR-determined scar distribution can be used to predict inducibility of VT in patients with ischemic or non-ischemic cardiomyopathy [4,18,19].

4.3. CE-MRI-based scar characterization and ablation success

Our study expanded our understanding of the utility of CE-MRI in VT ablation. A relatively large LV endocardial scar zone to total LV myocardial scar zone ratio predicted successful VT ablation via

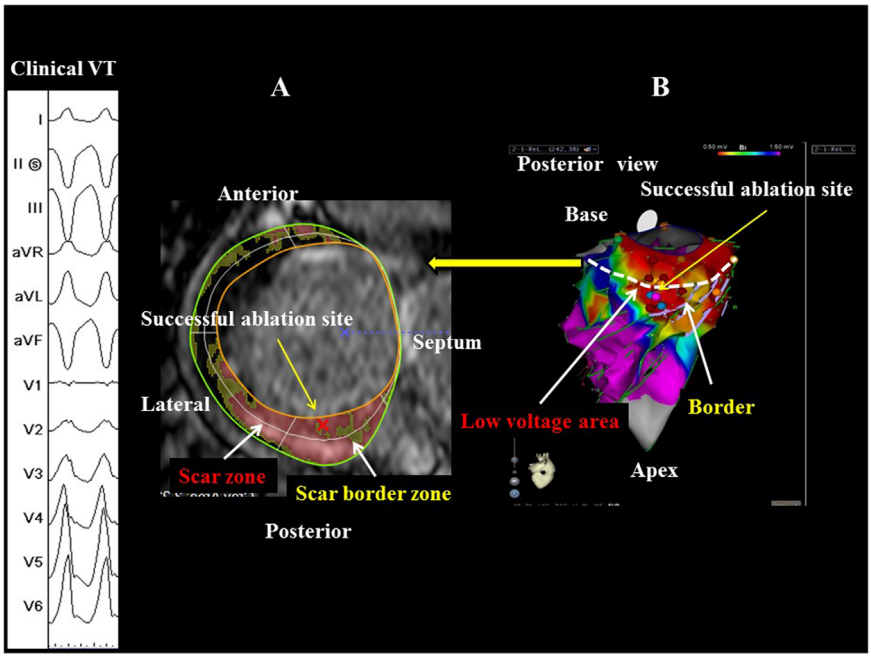

Fig. 5. Electrocardiogram, CE-MR image, and 3D endocardial LV voltage map in a case of sarcoidosis wherein LV ablation was successful via the endocardial approach. The VT morphology on the 12-lead ECG shows positive precordial QRS concordance and a superior axis, suggesting the VT origin at the base of the posterior LV. (A) The scar and scar border zones at the posterior LV are delineated on a short-axis slice of a 2D CE-MR image obtained at the LV base. (B) A successful ablation site is noted at the same place on the 3D endocardial LV voltage map. Dotted line indicates the line corresponding to the short-axis slice of the 2D CE-MR image in (A).

the LV endocardial side, and most successful VT ablation sites were located adjacent to scar border zones. VT origins exist at a critical isthmus often located in narrow scar border zones that can form between the scar zone and healthy myocardium, within or between two neighboring scar zones, or between the scar and an anatomical boundary, such as mitral/tricuspid valve [1–3]. Therefore, the substrate for the VT origin is related to the balance between the scar border and scar zones and healthy myocardium, but the coexistence of large scar zones is a necessary and sufficient condition to form a critical isthmus for VT. These and our findings suggest that the chance of these anatomical conditions to form the critical VT isthmus on the endocardial LV side may be increased by a larger distribution of scar zones on that side, rather than the extent of the scar border zones. Mapping and ablation of VT remains challenging because the VT origin is often in the endocardial side in patients with ischemic cardiomyopathy, but in the epicardial side or within the LV wall in some with non-ischemic cardiomyopathy [3]. Our finding highlights that CE-MRI can help guide decision-making, i.e., deciding whether to attempt an epicardial approach for VT catheter ablation [20]. Several recent studies have correlated the CE-MRI-derived scar zone and scar zone identified by 3D electro-anatomical mapping (EAM). Scar zones identified by CE-MRI correlate well with 3D EAM-derived-scar zones defined by bipolar voltage amplitudes of 1.3–1.5 mV [20–24], and in other studies, 3D EAM-derived scar zones defined by bipolar voltage amplitudes of $\leq$0.5 mV [25,26]. However, a mismatch was found between the EAM- and CE-CMR-derived scar zones in 33% of patients in one study [21].

Several groups have further assessed the relationship between the VT origin and CE-MRI-derived scar characteristics [24–26]. Desjardins et al. [24] reported that VT isthmus sites, the majority of which were identified by pace mapping, had a mean bipolar voltage of 0.6 ± 0.9 mV and corresponded to core scar regions or scar border zones found on CE-MR images by means of post-procedural image integration. Of importance in their study, no isthmus could be identified for a third of the induced VTs. Another group of investigators reported that they identified the critical isthmuses of VTs at a higher rate with CE-MRI [25] than that reported by Desjardins et al. [24]. The most recent of these studies yielded lower identification rates of 74% for the critical isthmus and 50% for conducting channels already identified on EAM [26]. These studies and ours were retrospective assessments, and thus, CE-MRI has potential for identifying the scar zone or scar border zone related to the VT reentrant circuit. Nonetheless, the image resolution needs to be improved, and refining the thresholding technique or integration technique is needed so that the data correspond to EAM data. CE-MRI can be currently used in combination with the VT morphology or conventional mapping techniques to identify landmarks of critical sites of the reentrant circuits for scar-related VT.

4.4. Limitations

Our study was limited by the number of patients included, and this prevented us from performing a multivariate analysis. Another important limitation was that we did not directly analyze the correlation between the scar or scar border zones derived from CE-MRI and low voltage zones identified by 3D EAM because the software that was available to us could not integrate CE-MRI and EAM data. However, we characterized the successful ablation sites identified on 3D electroanatomic maps using CE-MRI, though only retrospectively. Epicardial mapping from within the pericardial space was not performed in all patients in whom endocardial ablation was unsuccessful. Therefore, we could not identify the exact VT origin, or whether it was intramural or epicardial, in 11 patients in the unsuccessful ablation group. Finally, ablation success was not defined by the ultimate clinical outcomes as VT recurrences after ablation because we focused on the direct association between the MRI-derived scar formation and elimination of arrhythmogenic VT substrates by ablation from the endocardial side.

5. Conclusions

CE-MRI is useful for characterizing the scar and scar border zones that are susceptible to VT during programmed ventricular stimulation. A relatively large CE-MRI-derived scar on the endocardial LV side predicted successful VT ablation via the endocardium, with most successful VT ablation sites located adjacent to scar border zones. We expect CE-MRI to prove useful in preprocedural planning for catheter ablation of VT.

Disclosures

All authors declare no conflict of interest related to this study.

Acknowledgments

The authors thank Ms. Wendy Alexander-Adams and Mr. Martin John for their encouragement and assistance with the reporting of our findings in English.

Appendix A. Supplementary material

Supplementary data associated with this article can be found in the online version at http://dx.doi.org/10.1016/j.joa.2016.11.001.

References

[1] Stevenson WG, Khan H, Sager P, et al. Identification of the reentry circuit sites during catheter mapping and radiofrequency ablation of ventricular tachycardia late after myocardial infarction. Circulation 1993;88(4 Pt 1):1647–70.
[2] Soejima K, Stevenson WG, Maisel WH, et al. Electrically unexcitable scar mapping based on pacing threshold for identification of the reentry circuit isthmus. Circulation 2002;106:1678–83.
[3] Wilber DJ. Ablation of the epicardial substrate in ventricular tachycardia associated with structural heart disease: outside in or inside out? J Am Coll Cardiol 2014;63:1427–9.
[4] Schmidt A, Azevedo CF, Cheng A, et al. Infarct tissue heterogeneity by magnetic resonance imaging identifies enhanced cardiac arrhythmia susceptibility in patients with left ventricular dysfunction. Circulation 2007;115:2006–14.
[5] Spiewak M, Malek LA, Misko J, et al. Comparison of different quantification methods of late gadolinium enhancement in patients with hypertrophic cardiomyopathy. Eur J Radiol 2010;74:149–53.
[6] Neizel M, Katoh M, Schade E, et al. Rapid and accurate determination of relative infarct size in humans using contrast-enhanced magnetic resonance imaging. Clin Res Cardiol 2009;98:319–24.
[7] Amado LC, Gerber BL, Gupta SN, et al. Accurate and objective infarct sizing by contrast-enhanced magnetic resonance imaging in a canine myocardial infarction model. J Am Coll Cardiol 2004;44:2383–9.
[8] Beek AM, Bondarenko O, Afsharzada F, et al. Quantification of late gadolinium enhanced CMR in viability assessment in chronic ischemic heart disease: a comparison to functional outcome. J Cardiovasc Magn Reson 2009;11:6.
[9] Flett AS, Hasleton J, Cook C, et al. Evaluation of techniques for the quantification of myocardial scar of differing etiology using cardiac magnetic resonance. JACC Cardiovasc Imaging 2011;4:150–6.
[10] Hsu LY, Natanzon A, Kellman P, et al. Quantitative myocardial infarction on delayed enhancement MRI. Part I: animal validation of an automated feature analysis and combined thresholding infarct sizing algorithm. J Magn Reson Imaging 2006;23:298–308.
[11] Yan AT, Shayne AJ, Brown KA, et al. Characterization of the peri-infarct zone by contrast-enhanced cardiac magnetic resonance imaging is a powerful predictor of post-myocardial infarction mortality. Circulation 2006;114:32–9.
[12] Klem I, Weinsaft JW, Bahnson TD, et al. Assessment of myocardial scarring improves risk stratification in patients evaluated for cardiac defibrillator implantation. J Am Coll Cardial 2012;60:408–20.
[13] Das MK, Khan B, Jacob S, et al. Significance of a fragmented QRS complex versus a Q wave in patients with coronary artery disease. Circulation 2006;113:2495–501.
[14] Kramer C, Barkhausen J, Flamm SD, et al. Standardized cardiovascular magnetic resonance imaging (CMR) protocols, Society for Cardiovascular Magnetic Resonance: board of Trustees Task Force on Standardized Protocols. J Cardiovasc Magn Reson 2008;10:35.
[15] Yao JA, Jussain W, Patel P, et al. Remodeling of gap junctional channel function in epicardial border zone of healing canine infarcts. Circ Res 2003;2:437–43.
[16] de Bakker JM, van Capelle FJ, Janse MJ, et al. Reentry as a cause of ventricular tachycardia in patients with chronic ischemic heart disease: electrophysiologic and anatomic correlation. Circulation 1988;77:589–606.
[17] Verma A, Marrouche NF, Schweikert RA, et al. Relationship between successful ablation sites and the scar border zone defined by substrate mapping for ventricular tachycardia post-myocardial infarction. J Cardiovasc Electrophysiol 2005;16:465–71.
[18] Bello D, Fieno DS, Kim RJ, et al. Infarct morphology identifies patients with substrate for sustained VT. J Am Coll Cardiol 2005;45:1104–8.
[19] Nazarian S, Bluemke DA, Lardo AC, et al. Magnetic resonance assessment of the substrate for inducible ventricular tachycardia in non-ischemic cardiomyopathy. Circulation 2005;112:2821–5.
[20] Bogun FM, Desjardins B, Good E, et al. Delayed-enhanced magnetic resonance imaging in nonischemic cardiomyopathy: utility for identifying the ventricular arrhythmia substrate. J Am Coll Cardiol 2009;53:1138–45.
[21] Codreanu A, Odille F, Aliot E, et al. Electroanatomic characterization of post-infarct scars comparison with 3-dimensional myocardial scar reconstruction based on magnetic resonance imaging. J Am Coll Cardiol 2008;52:839–42.
[22] Wijnmaalen AP, van der Geest RJ, van Huls van Taxis CF, et al. Head-to-head comparison of contrast-enhanced magnetic resonance imaging and electroanatomical voltage mapping to assess post-infarct scar characteristics in patients with ventricular tachycardias: real-time image integration and reversed registration. Eur Heart J 2011;32:104–14.
[23] Andreu D, Berruezo A, Ortiz-Pérez JT, et al. Integration of 3D electroanatomic maps and magnetic resonance scar characterization into the navigation system to guide ventricular tachycardia ablation. Circ Arrhythm Electrophysiol 2011;4:674–83.
[24] Desjardins B, Crawford T, Good E, et al. Infarct architecture and characteristics on delayed enhanced magnetic resonance CE-MRI integration during VT ablation imaging and electroanatomic mapping in patients with postinfarction ventricular arrhythmia. Heart Rhythm 2009;6:644–51.
[25] Perez-David E, Arenal A, Rubio-Guivernau JL, et al. Noninvasive identification of ventricular tachycardia-related conducting channels using contrast-enhanced magnetic resonance imaging in patients with chronic myocardial infarction: comparison of signal intensity scar mapping and endocardial voltage mapping. J Am Coll Cardiol 2011;57:184–94.
[26] Fernández-Armenta J, Berruezo A, Andreu D, et al. Three-dimensional architecture of scar and conducting channels based on high resolution ce-CMR: insights for ventricular tachycardia ablation. Circ Arrhythm Electrophysiol 2013;6:528–37.